Pharmacology Research & Perspectives

ORIGINAL ARTICLE OPEN ACCESS

NMDA Receptor–Mediated Ca^{2+} Flux Attenuated by the NMDA Receptor/TRPM4 Interface Inhibitor Brophenexin

Jordan Casby | Benjamin M. Gansemer | Stanley A. Thayer

Department of Pharmacology, University of Minnesota Medical School, Minneapolis, Minnesota, USA

Correspondence: Stanley A. Thayer (sathayer@umn.edu)

Received: 16 May 2024 | **Revised:** 12 August 2024 | **Accepted:** 1 November 2024

Funding: This work was made possible by the National Institutes of Health grant from the National Institute on Drug Abuse [Grant DA07304] to S.A.T.

Keywords: brophenexin | Ca^{2+} signaling | excitotoxicity | NMDAR | TRPM4

ABSTRACT

Transient receptor potential melastatin-4 (TRPM4) forms a complex with *N*-methyl-D-aspartate receptors (NMDARs) that facilitates NMDAR-mediated neurotoxicity. Here we used pharmacological tools to determine how TRPM4 regulates NMDAR signaling. Brophenexin, a compound that binds to TRPM4 at the NMDAR binding interface, protected hippocampal neurons in culture from NMDA-induced death, consistent with published work. Brophenexin (10 μM) reduced NMDA-evoked whole-cell currents recorded at 22°C by 87% ± 14% with intracellular Ca^{2+} chelated to prevent TRPM4 activation. Brophenexin inhibited NMDA-evoked currents recorded in Na^{+}-free solution by 87% ± 13%, suggesting that brophenexin and TRPM4 modulate NMDAR function. Incubating cultures in Mg^{2+}-free buffer containing tetrodotoxin, 6-cyano-7-nitroquinoxaline-2,3-dione, and bicuculline for 30 min inhibited NMDA-evoked increases in intracellular Ca^{2+} concentration ($[Ca^{2+}]_i$) recorded at 22°C by 50% ± 18% and prevented inhibition by brophenexin. In the absence of these inhibitors, brophenexin inhibited the NMDA-evoked response by 51% ± 16%. Treatment with the TRPM4 inhibitor 4-chloro-2-(1-naphthyloxyacetamido)benzoic acid (NBA; 10 μM) increased NMDA-evoked Ca^{2+} influx by 90% ± 15%. Increasing extracellular NaCl to 237 mM, a treatment that activates TRPM4, inhibited the NMDA-evoked increase in $[Ca^{2+}]_i$ by a process that occluded the inhibition produced by brophenexin and was prevented by NBA. In recordings performed at 32°C–34°C, brophenexin inhibited the NMDA-evoked $[Ca^{2+}]_i$ response by 42% ± 10% but NBA was without effect. These results are consistent with a model in which TRPM4 interacts with NMDARs to potentiate Ca^{2+} flux through the NMDAR ion channel and thus provides a potential mechanism for the neuroprotection afforded by NMDAR/TRPM4 interface inhibitors such as brophenexin.

1 | Introduction

N-methyl-D-aspartate receptors (NMDARs) play an essential role in the synaptic plasticity that underlies learning and memory [1]. Excessive Ca^{2+} influx via NMDARs triggers excitotoxicity that contributes to many neurodegenerative diseases including Alzheimer's disease, Parkinson's disease, and Huntington's disease, as well as stroke and traumatic brain injuries [2]. NMDARs found at the synapse (sNMDAR) are pro-survival and contribute to synaptic plasticity while extrasynaptic

Abbreviations: AUC, area under the curve; BAPTA, 1,2-bis(*o*-aminophenoxy)ethane-*N*,*N*,*N*′,*N*′-tetraacetic acid; Bic, bicuculline; BPN, brophenexin, *N*′-[(3-bromophenyl)methyl]-*N*′-ethylethane-1,2-diamine;dihydrochloride; CNQX, 6-cyano-7-nitroquinoxaline-2,3-dione; DIV, day in vitro; DMEM, Dulbecco's modified Eagle medium; F_{340}/F_{380}, ratio of fura-2 fluorescence excited at 340 nm to that excited at 380 nm; $GABA_AR$, γ-aminobutyric acid type A receptor; HBSS, Hanks' balanced salt solution; HHSS, HEPES-buffered Hanks' salt solution; I_{NMDA}, NMDA-evoked current; NBA, 4-chloro-2-(2-(naphthalene-1-yloxy) acetamido) benzoic acid; NMDA, *N*-methyl-D-aspartate; NMDAR, *N*-methyl-D-aspartate receptor; NMDG, *N*-methyl-D-glucamine; ROI, region of interest; TRPM4, transient receptor potential cation channel melastatin-4; TTX, tetrodotoxin; $[Ca^{2+}]_i$, intracellular-free Ca^{2+} concentration.

Jordan Casby and Benjamin M. Gansemer contributed equally to this work.

NMDARs (esNMDAR) are responsible for signaling that leads to mitochondrial dysfunction and cell death [3, 4]. NMDARs that contain the GluN2A subunit are primarily synaptic while GluN2B-containing NMDARs are primarily extrasynaptic, but this separation is not absolute and changes during development and activity [5]. Thus, selective pharmacological targeting of pathological NMDAR signaling while sparing physiological signaling has proven difficult.

An important discovery with the potential to enable selective pharmacological targeting of excitotoxic NMDAR signaling was the finding that the ion channel transient receptor potential melastatin-4 (TRPM4) forms a complex with esNMDAR, and this complex is necessary for NMDAR-mediated neurotoxicity [6]. Molecular characterization of the NMDAR/TRPM4 interface identified TwinF as the region on TRPM4 that binds to the NMDAR. The TwinF peptide acts as a competitive inhibitor of complex formation and in so doing protects from NMDAR-mediated toxicity in vitro and from stroke-mediated brain damage in vivo [6].

TRPM4 is permeable to monovalent cations, primarily Na^+, and it is activated by increases in the intracellular free Ca^{2+} concentration ($[Ca^{2+}]_i$) [7], mechanical stress [8], decreases in cellular ATP [9], and changes in temperature [10, 11]. TRPM4 is widely expressed and has been implicated in cardiac arrhythmias and several types of cancer [12, 13]. Na^+ influx through TRPM4 depolarizes the membrane potential, which dysregulates Ca^{2+} homeostasis in cardiac and cancer cells [12, 13]. Knockout of *Trpm4* impaired long-term potentiation (LTP) of synaptic transmission in the hippocampus in a manner rescued by facilitating NMDAR activation [14]. Inhibition of TRPM4 is neuroprotective in models of cerebral edema [15], aneurysmal subarachnoid hemorrhage [16], and experimental autoimmune encephalomyelitis [17], making it a potential therapeutic target for neurotoxic conditions.

Several inhibitors of TRPM4 function have been developed. 9-Phenanthrol is a widely used inhibitor of TRPM4, but it lacks specificity and potency [18]. Inhibitors with increased potency and specificity were identified in a functional screen [19], and two compounds with sub-micromolar potency, 4-chloro-2-(2-chlorophenoxyacetamido)benzoic acid (CBA) and 4-chloro-2-(1-naphthyloxyacetamido)benzoic acid (NBA), have been described [18]. NBA is more potent than CBA in rodent models, which determined its use in this study [20]. While small molecule inhibitors of TRPM4 show therapeutic promise, the ubiquitous expression of TRPM4 could lead to on-target adverse effects, again showing the need for highly selective inhibitors.

Yan et al. [6] recently described a new class of small molecules that bind to the TwinF site on TRPM4 blocking complex formation between esNMDARs and TRPM4. A prototype NMDAR/TRPM4 interface inhibitor described as "compound 8" and also known as brophenexin (BPN) (PubChem CID 138040845) was found to attenuate NMDA-evoked depolarization of mitochondrial membrane potential and protect from NMDA-induced neurotoxicity. BPN provided protection from stroke-induced brain damage, and a structural analog with reduced long-term in vivo adverse effects, N′-[(3-chlorophenyl)methyl]-N′-ethylethane-1,2-diamine (FP802), was effective in a mouse model of amyotrophic lateral sclerosis (ALS) [21]. NMDAR/TRPM4 interface inhibitors represent an exciting new target for neuroprotective drugs [22]. However, it is unclear how TRPM4 contributes to cell death signaling by esNMDARs and why disrupting the NMDAR/TRPM4 complex is therapeutic.

Here, we replicated the neuroprotective effects of BPN described by Yan et al. [6] and tested the hypothesis that BPN inhibits Ca^{2+} influx via NMDARs. Treating rat hippocampal cultures with BPN inhibited NMDA-evoked increases in $[Ca^{2+}]_i$ in a manner blocked by the TRPM4 inhibitor NBA. NBA increased NMDA-evoked $[Ca^{2+}]_i$ responses. This work shows that drugs that bind TRPM4 can potentiate or inhibit NMDAR function.

2 | Materials and Methods

2.1 | Reagents

Materials were obtained from the following sources: propidium iodide (P1304MP), Fura-2 AM (F1201), DMEM (31053), HBSS (14175), fetal bovine serum (26140), horse serum (16050), penicillin/streptomycin (15140), and poly-D-lysine (A3890401) were from Thermo Fisher Scientific (Carlsbad, CA, USA); NMDA (M3262), glycine (G6388), MK-801 (M107), CNQX (C239), FCCP (C2920), laminin (SIAL-L2020), AP-5 (A5282), HEPES (H4034), N-methyl-D-glucamine (NMDG) (M2004), mannitol (M1902), and DMSO (276855) were from Millipore Sigma (St. Louis, MO, USA); pluronic f-127 (20050) was from AAT Bioquest (Pleasanton, CA, USA); bicuculline (10910) was from Tocris-Biotechne (Minneapolis, MN, USA); Tetrodotoxin (TTX) (CAYM-14964-1) was from Cayman Chemical (Ann Arbor, MI, USA); NBA (lot numbers 144 372 and 246 952) and BPN (lot numbers 002776824 U and 257 289) were from MedChemExpress (Monmouth Juncton, NJ, USA); 24-well plates (P24G-1.5-10-F) were from MatTek (Ashland, MA, USA).

2.2 | Cell Culture

All animal care and experimental procedures were performed following the Guide for the Care and Use of Laboratory Animals published by the U.S. National Institutes of Health. Ethical approval was granted by the Institutional Animal Care and Use Committee of the University of Minnesota (protocol 1612-34372A). Rat hippocampal cultures were prepared as previously described [23] with minor modifications. Briefly, pregnant Sprague–Dawley rats (RGD_737891; Charles River, Wilmington, MA, USA) were euthanized by CO_2 inhalation, embryonic day 17 fetuses of both sexes were decapitated with sharp scissors, and hippocampi dissected and placed in ice-cold Ca^{2+}- and Mg^{2+}-free Hanks' balanced salt solution (HBSS). HBSS was replaced with Dulbecco's modified Eagle medium (DMEM) supplemented with 10% fetal bovine serum and penicillin/streptomycin (100 U/mL and 100 mg/mL, respectively) and the cell suspension triturated with flame-narrowed Pasteur pipets to dissociate cells. Glass coverslips (number 1.5, 25 mm diameter, catalog number GG-25-15, Neuvitro Corporation, Camas, WA, USA) or 24-well plates (MatTek, Ashland, MA,

USA) were prepared in advance by coating with phosphate-buffered saline containing 9 μg/mL high molecular weight poly-D-lysine and 0.4 μg/mL laminin. The coverglass or well bottom in a 24-well plate was completely covered in coating solution for 1 h, washed with water, allowed to dry for 1 h, and then cell suspension was plated as a 200 μL droplet at a density of 150 000 cells per coverslip or a 200 μL droplet at a density of 75 000 cells per well. Cultures were maintained at 37°C in a humidified atmosphere containing 10% CO_2. On day in vitro (DIV) 1 and 8, three-quarters of the medium was replaced with DMEM supplemented with 10% horse serum and penicillin/streptomycin. Cells used in these experiments were cultured without mitotic inhibitors for 14–15 DIV resulting in a mixed glial-neuronal culture consisting of 18% ± 2% neurons, 70% ± 3% astrocytes, and 9% ± 3% microglia as indicated by immunocytochemistry [24].

2.3 | Whole-Cell Patch-Clamp Recordings

NMDA-evoked currents were recorded at room temperature (22°C) as previously described [25]. Glass pipettes were pulled to a resistance of 3–7 MΩ when filled with a recording solution containing (in mM): 145 K-gluconate, 10 HEPES, 5 MgATP, 0.5 NaGTP, and 10 BAPTA, pH 7.2 with KOH, 310 mOsm. Cells were bathed in an extracellular solution containing (in mM): 125 NaCl, 2 KCl, 2 CaCl, 25 HEPES, 30 glucose, and 2 MgCl (MgCl was omitted for Mg-free solutions), pH 7.35 with NaOH, 315 mOsm. Cells were voltage clamped at −60 mV and washed for 60 s in Mg^{2+}-free solution containing 3 μM CNQX, 100 nM TTX, 15 μM glycine, and 10 μM bicuculline. NMDA (20 μM) was then applied for 60 s via superfusion, followed by washout in Mg^{2+}-free solution. Each cell received 2 applications of NMDA, with at least 5 min between applications. The first application for all cells was NMDA alone. For NMDA+BPN recordings, the solution for the washout period after the first NMDA application contained 10 μM BPN. The BPN then remained in the bath during the second NMDA application. Steady-state NMDA current amplitudes were measured from a 10 s average after 30 s of exposure to NMDA. A 30-s average baseline measurement was taken before each NMDA application and subtracted from the steady-state amplitude. For Na^+-free recordings, an approach similar to that described in [26] was used. NaCl was replaced with 125 mM NMDG in the extracellular solution and $CaCl_2$ increased to 10 mM. For the intracellular solution, K-gluconate was replaced with 145 mM NMDG, NaGTP was omitted, and the pH of the solution was adjusted with gluconic acid. Additionally, cells were voltage-clamped at −70 mV and each cell received only one application of 20 μM NMDA.

2.4 | $[Ca^{2+}]_i$ Imaging

Fura-2-based $[Ca^{2+}]_i$ imaging was performed as previously described [27]. Briefly, a coverslip with adhered cells was incubated in HEPES-buffered Hanks' salt solution (HHSS) containing 5 μM Fura-2 AM in 0.1% pluronic acid for 30–60 min at 37°C. The coverslip was then washed in HHSS for 15–30 min and placed in a recording chamber [28]. HHSS contained the following (in mM): HEPES 20, NaCl 137, $CaCl_2$ 1.3, $MgSO_4$ 0.4, $MgCl_2$ 0.5, KCl 5.0, KH_2PO_4 0.4, Na_2HPO_4 0.6, $NaHCO_3$ 3.0, and glucose 5.6.

The recording chamber was placed on the stage of an Olympus IX71 inverted microscope and cells were viewed with an Olympus 40× oil immersion objective (UApo 340, 1.35 numerical aperture). The excitation wavelength was selected with a galvanometer-driven monochromator (8-nm slit width) coupled to a 75-W xenon arc lamp (Optoscan; Cairn Research). Fluorescence images (510/40 nm) were projected onto a cooled charge-coupled device camera (Cascade 512B; Roper Scientific) controlled by MetaFluor software (Molecular Devices).

$[Ca^{2+}]_i$ was monitored using sequential excitation of fura-2 at 340 and 380 nm; image pairs were collected every 1 s. Cells were superfused at a rate of 1–2 mL per min from gravity-fed reservoirs containing HHSS with the indicated drugs. For recordings performed at 32°C–34°C, temperature was regulated with a temperature controller (TC-324C Warner Instruments, Holliston, MA, USA), the HHSS flowing into the chamber was preheated with an inline heater, and bath temperature monitored with a thermistor placed in the recording chamber. The microscope objective was held at 37°C using a lens heater (Tokai Hit, Bala Cynwyd, PA, USA). During experimental recordings, cells were superfused for 1 min in Mg^{2+}-free HHSS, and then responses evoked by 30 s superfusion with Mg^{2+}-free HHSS that contained 20 μM NMDA and 200 μM glycine.

2.5 | Neuronal Death Assay

Neurons were maintained in 24-well plates as described above. Experiments were performed in triplicate in 3 separate platings of cells. Drug treatments were applied 1 h before the challenge with either a media exchange (control) or the challenge with Mg^{2+}-free HHSS that contained 20 μM NMDA and 200 μM glycine. Propidium iodide (5 μM) was added to all wells. Cultures were imaged using both differential interference contrast and epi-fluorescence (561 nm excitation, 600 nm emission 50 nm bandpass) 24 h after NMDA treatment using a Nikon 20× air objective (PlanApo, 0.75 numerical aperture) on a Nikon Ti-E inverted microscope (Nikon, Melville, NY, USA). Image files were coded, and neurons were counted by an observer blinded to treatment. The ratio of neurons that took up propidium iodide relative to the total number of neurons in the field was reported as percent neuronal death.

2.6 | Experimental Design and Statistical Analysis

Sample sizes for the cell death assay were based on published work using a similar approach [6], as were the sample sizes for I_{NMDA} recordings [26] and $[Ca^{2+}]_i$ recordings [29].

I_{NMDA} experiments were analyzed using pCLAMP v.11.0. Cells were only included for analysis if the initial access resistance (R_A) was < 35 MΩ and did not change by more than 25% over the course of the recording.

$[Ca^{2+}]_i$ was calculated using MetaFluor software (Molecular Devices). The neuronal cell body was selected as the region of interest for all recordings. All neurons within the imaging field were included in the analysis and no exclusions were made. For time course experiments, coverslips from the same cell culture

plating were treated in parallel and each coverslip was imaged only once. $[Ca^{2+}]_i$ values are reported as background corrected 340 nm/380 nm fluorescence intensity ratios (F_{340}/F_{380}).

Statistical analyses were performed using Prism 10 (GraphPad Software). Primary neuronal cultures were derived from 8 to 12 animals with a unique network forming on each coverslip; thus, each recording from a single coverslip constitutes a biological replicate. All data were tested for deviation from a normal distribution with the D'Agostino–Pearson test. For experiments with two groups, a Student's *t*-test was performed, or if variances were not equal a Welch's *t*-test was used. For experiments with 3 or more groups, a one-way or two-way ANOVA was performed with Tukey's post hoc test. Statistical significance was defined as $p < 0.05$. All error bars are shown as SD unless otherwise specified.

2.7 | Nomenclature of Targets and Ligands

Key protein targets and ligands in this article are hyperlinked to corresponding entries in http://www.guidetopharmacology.org, the common portal for data from the IUPHAR/BPS Guide to PHARMACOLOGY [30], and are permanently archived in the Concise Guide to PHARMACOLOGY 2023/24: Ion Channels [31].

3 | Results

3.1 | BPN Protects From NMDA-Evoked Excitotoxicity

Previous research has shown that BPN reduces NMDA-evoked neuronal death [6]. We confirmed that BPN protects from NMDA-evoked toxicity using a propidium iodide uptake assay to identify dead neurons in rat primary hippocampal cultures (Figure 1A). Treatment with 20 μM NMDA for 24 h significantly increased the percentage of neurons that died as determined by uptake of propidium iodide (267% ± 34%) (Figure 1B). Cultures pretreated for 1 h with either 10 μM or 100 μM BPN exhibited, respectively, a 24% ± 5% or 24% ± 7% reduction in neuronal death relative to those treated with NMDA alone showing a partial protective effect (Figure 1B).

3.2 | BPN Inhibits NMDA-Evoked Currents

Whole-cell patch clamp recordings of NMDA-evoked currents (I_{NMDA}) at room temperature were used to assess BPN's effect on NMDAR channel activity. Each cell was challenged twice with 20 μM NMDA and 200 μM glycine in Mg^{2+}-free buffer enabling the use of the first response as control ($I_{NMDA} = 8.01 \pm 0.85$ pA/pF). I_{NMDA} were reproducible with the second response decreasing by only 5% ± 23% (Figure 2A). In contrast, treatment with BPN for 5 min before the second NMDA application reduced I_{NMDA} by 87% ± 14% (Figure 2B). Thus, I_{NMDA} was reduced significantly by treatment with BPN relative to untreated cells (Figure 2C). The magnitude of BPN inhibition and the presence of BAPTA in the intracellular solution suggest that TRPM4 modulates NMDAR function.

To explicitly address the question of whether the effects of BPN were dependent on Na^+ flux, whole-cell patch clamp recordings of I_{NMDA} were recorded in Na^+-free extracellular solution using a previously published protocol [26] in which *N*-methyl-D-glucamine (NMDG) was substituted for Na^+ and Ca^{2+} was increased to 10 mM to serve as a charge carrier. The cells were not stable in the NMDG recording solution for prolonged periods, so the paired protocol was not used and instead, I_{NMDA} is presented

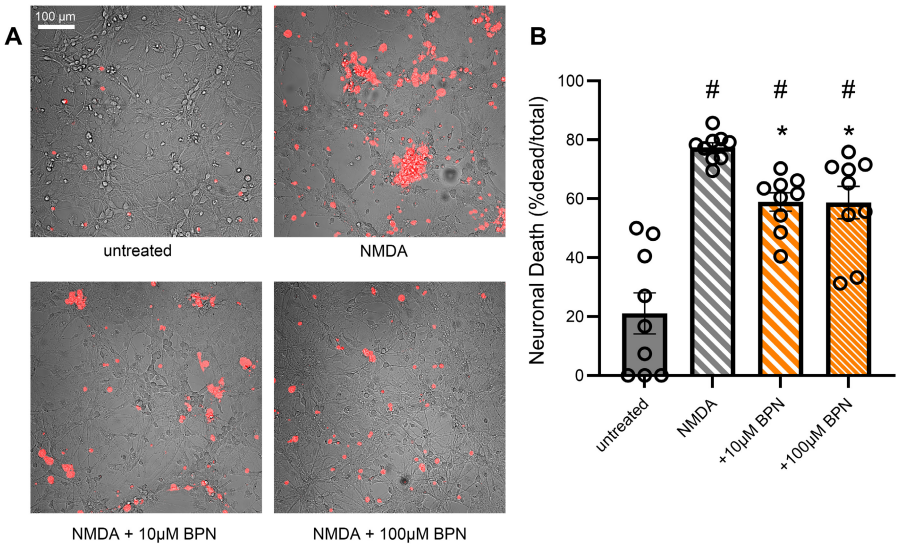

FIGURE 1 | The effects of BPN on NMDA-evoked neurotoxicity. Neuronal death was measured using a propidium iodide uptake assay. (A) Representative images show propidium iodide fluorescence (red) overlaid on a differential interference contrast image of microscopic fields. (B) Bar graph displays neuronal death as a percentage of total neurons present in the field. Cultures were untreated (solid bar) or treated with 20 μM NMDA and 200 μM glycine in Mg^{2+}-free HHSS (hatched bars) for 24 h. Orange bars indicate cultures pretreated for 1 h with 10 μM (thick hatches) or 100 μM (thin hatches) BPN before and during NMDA exposure. One-way ANOVA: $F_{(3,32)} = 24.40$, $p < 0.0001$. *$p < 0.05$ relative to NMDA treated; $^{\#}p < 0.0001$ relative to untreated, with Tukey's post hoc test. Data presented as mean ± SD. Individual points are means determined from a single well. Each treatment was tested in 3 wells on 3 separate platings of cells ($n = 9$ wells).

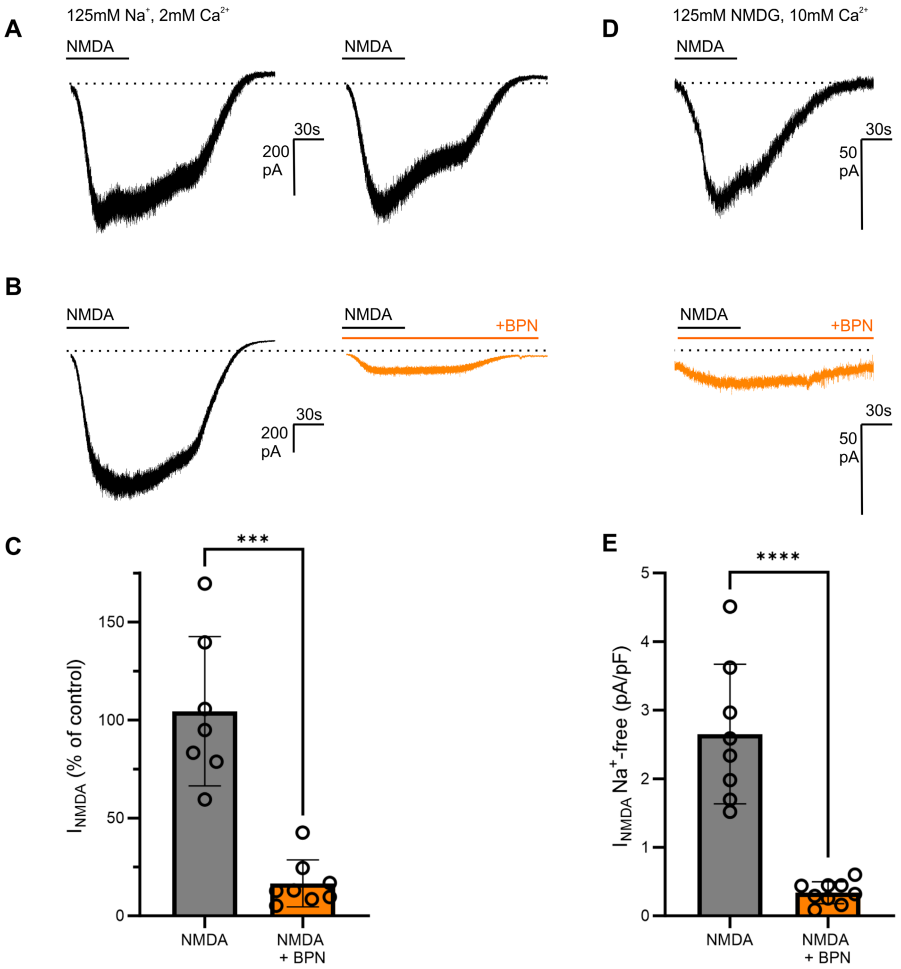

FIGURE 2 | Effect of BPN on I_{NMDA}. (A, B) Representative traces show paired whole-cell NMDA-evoked currents. Neurons were voltage clamped at −60 mV at room temperature (22°C) and currents evoked by 20 μM NMDA and 200 μM glycine in Mg^{2+}-free recording buffer applied by bath perfusion at the times indicated by the black horizontal bars. The first application of NMDA was applied to an untreated cell (left trace). A second application of NMDA was applied 5 min after incubation in extracellular solution containing vehicle (A) or 10 μM BPN (B *orange trace*). Scale bars, 200 pA, 30 s. (C) Bar graph summarizes the magnitude of the second I_{NMDA} as a percentage of the first ($100 \times I_{NMDA}$ 2/I_{NMDA} 1). I_{NMDA} was significantly reduced when the second NMDA application occurred in the presence of BPN. Welch's *t*-test: $T_{(5.847)} = 7.034$, $^{***}p < 0.001$. Data presented as mean ± SD. Individual points = individual cells. (D) Representative traces show whole-cell I_{NMDA} evoked in Mg^{2+}- and Na^{+}-free extracellular solution containing 10 mM Ca^{2+} and using a K^{+}-free pipette solution. Neurons were voltage clamped at −70 mV and NMDA (20 μM) was applied as indicated by the black horizontal bars either alone (top) or in the presence of 10 μM BPN (bottom, *orange trace*). (E) Bar graph summarizes I_{NMDA} normalized to cell capacitance in the absence (gray bar) or the presence of BPN (orange bar). Student's *t*-test: $T_{(15)} = 6.750$, $^{****}p < 0.0001$. Data presented as mean ± SD. Individual points = individual cells.

as current densities. I_{NMDA} recorded in Na^{+}-free solution (2.65 ± 0.36 pA/pF) was reduced by 67% ± 15% (Figure 2D,E) relative to the more physiological solutions used in Figure 2A–C (Student's *t*-test: $t_{[21]} = 4.432$, $p = 0.0002$). However, 10 μM BPN remained effective. BPN reduced I_{NMDA} carried by Ca^{2+} by 87% ± 13%. Thus, BPN inhibits Ca^{2+} flux through the NMDAR independent of Na^{+} (Figure 2D,E).

3.3 | NMDA-Evoked Changes in $[Ca^{2+}]_i$ Are Sensitive to BPN and Pretreatment Time in TTX, CNQX, and Bic

A previous study found that BPN did not affect NMDA-evoked $[Ca^{2+}]_i$ responses [6], which does not reconcile with our finding that BPN inhibits I_{NMDA}. To investigate, cells were loaded with fura-2 AM for 30 min and then washed in Mg^{2+}-free HHSS containing the same channel blockers used to isolate I_{NMDA} (TTX, CNQX, and Bic) in patch-clamp experiments (Figure 2). The $[Ca^{2+}]_i$ was recorded using digital imaging and responses evoked by treatment with 20 μM NMDA and 200 μM glycine in Mg^{2+}-free HHSS for 30 s. NMDA-evoked responses were markedly reduced following 30 min incubation in the channel blockers (Figure 3). The reduction in response depended on the time the cells were incubated in Mg^{2+}-free HHSS containing TTX, CNQX, and Bic (Figure 3) and the inhibition occluded the inhibition produced by BPN (Figure 3D). Cultures pretreated with 10 μM BPN during the 30 min wash step in the presence of the channel blockers showed no difference in response magnitude relative to cells treated with Mg^{2+}-free HHSS and the channel blockers alone (Figure 3A,D). However, NMDA-evoked $[Ca^{2+}]_i$ responses in cells washed with the channel blockers for only

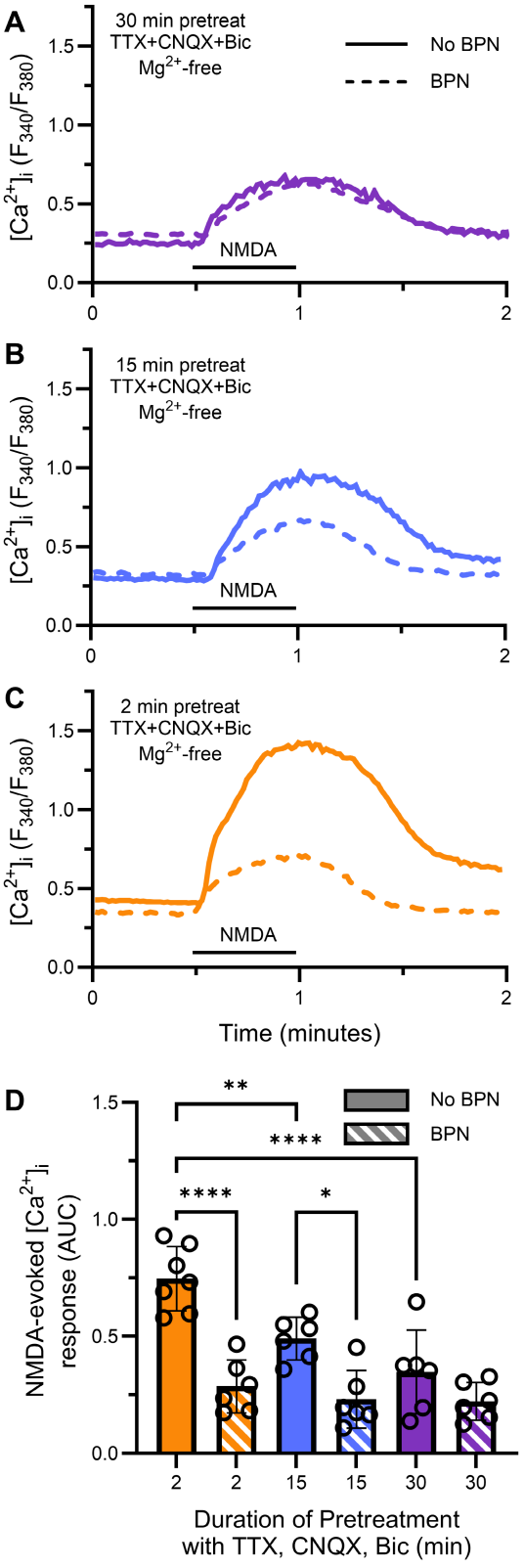

FIGURE 3 | The effects of time exposed to TTX, CNQX, Bic, and BPN on NMDA-evoked increases in $[Ca^{2+}]_i$. (A–C) Representative $[Ca^{2+}]_i$ recordings show average values from all cells in a single field. $[Ca^{2+}]_i$ was measured at room temperature (22°C) using fura-2-based digital imaging as described in Methods. Primary hippocampal cultures were loaded with fura-2AM (5 μM) for 30 min. Cells were mounted in the recording chamber and superfused with Mg^{2+}-free HHSS containing 100 nM TTX, 3 μM CNQX, and 10 μM bicuculline (Bic) in the absence (solid lines) or presence of 10 μM BPN (dashed lines) for 30 min (A), 15 min (B), or 2 min (C). NMDA (20 μM) and glycine (200 μM) were applied for 30 s by superfusion at the time indicated by the horizontal bar followed by Mg^{2+}-free HHSS containing TTX, CNQX, Bic. (D) Bar graph summarizes the area under the curve (AUC), determined by integrating the F_{340}/F_{380} ratio during the time of NMDA exposure and recovery. Treatment times of 30 min (purple), 15 min (blue), and 2 min (orange) correspond to the representative traces shown in (A–C). Treatment with BPN is indicated by the cross-hatched bars. A two-way ANOVA found a significant effect of incubation time ($F_{(2,31)} = 5.665$, $p = 0.008$), BPN treatment ($F_{(1,31)} = 46.73$, $p < 0.0001$), and a time x treatment interaction ($F_{(2,31)} = 11.13$, $p = 0.0002$). *$p < 0.05$, **$p < 0.01$, ***$p < 0.001$, ****$p < 0.0001$ with Tukey's post hoc test. No significant difference was found between groups treated with BPN regardless of incubation time nor was there a difference between 30 min incubation and 30 min incubation + BPN. Data presented as mean ± SD. Individual points are mean $[Ca^{2+}]_i$ values for all cells in a single field from a single coverslip.

2 min (Figure 3C,D) exhibited significantly larger $[Ca^{2+}]_i$ increases relative to those treated with the channel blockers for 15 (Figure 3B) or 30 min (Figure 3A). Furthermore, BPN inhibited the larger NMDA-evoked responses evoked after 15 (Figure 3B) or 2 min (Figure 3C) in Mg^{2+}-free HHSS containing TTX, CNQX, and Bic. Thus, BPN clearly inhibits NMDA-evoked $[Ca^{2+}]_i$ increases (Figure 3), consistent with the inhibition of I_{NMDA} observed in the patch-clamp experiments (Figure 2).

3.4 | NMDA-Evoked Changes in $[Ca^{2+}]_i$ Are Sensitive to $GABA_AR$ and NMDAR Antagonists

We next determined why treatment with the channel blockers TTX, CNQX, and Bic in Mg^{2+}-free HHSS altered NMDA-evoked $[Ca^{2+}]_i$ responses. We considered the individual channel blockers in the wash treatment. Removing Bic from the pretreatment wash and thus incubating the cultures in Mg^{2+}-free HHSS containing TTX and CNQX for 15 min restored the magnitude of the NMDA-evoked $[Ca^{2+}]_i$ response (Figure 4). This suggests that $GABA_AR$ inhibition partially occludes the effect of BPN. Because the time-dependent inhibition of the NMDA-evoked response produced by the Bic-containing wash was accompanied by an attenuated BPN-sensitive component of the increase in $[Ca^{2+}]_i$ (Figure 3), we considered the possibility that the Bic was activating TRPM4. To test this possibility, we pretreated the cells with Mg^{2+}-free HHSS containing TTX, CNQX, and Bic in the presence of the selective and potent TRPM4 inhibitor NBA [19]. NBA afforded no protection from the attenuation of the NMDA-evoked $[Ca^{2+}]_i$ response produced by 15 min treatment with Mg^{2+}-free HHSS containing TTX, CNQX, and Bic (Figure 4). These findings suggest that the reduction in NMDA-evoked $[Ca^{2+}]_i$ responses by bicuculline is independent of TRPM4 ion channel activity.

Because metabotropic activation of NMDARs can evoke Ca^{2+} influx by routes other than the NMDAR ion channel we confirmed that the increase in $[Ca^{2+}]_i$ evoked by 30 s treatment with 20 μM NMDA +200 μM glycine resulted from Ca^{2+} flux through the NMDAR by treating with the NMDAR antagonist MK801

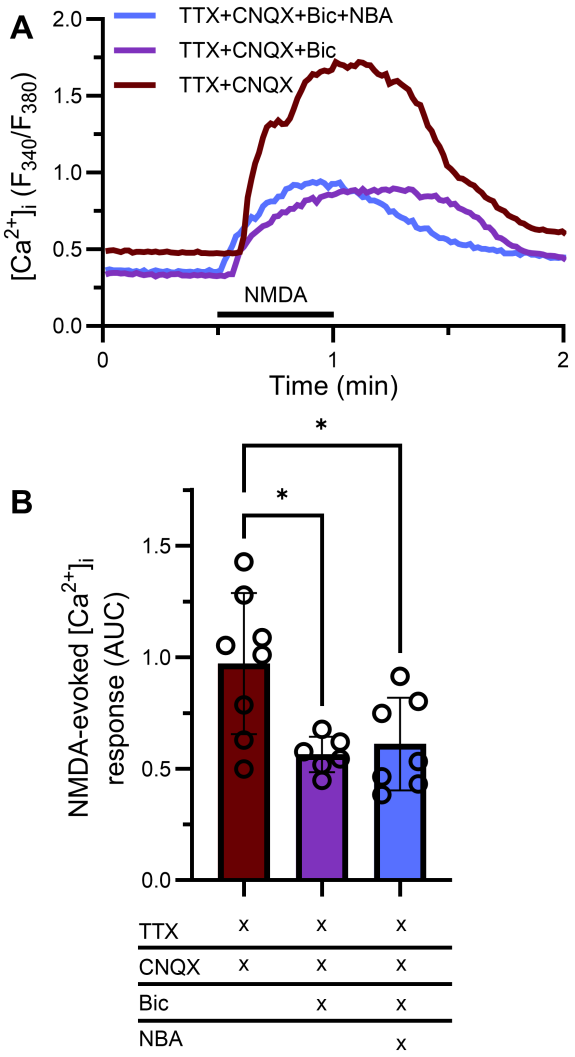

FIGURE 4 | The effects of TTX, CNQX, and Bic on NMDA-evoked increases in $[Ca^{2+}]_i$ (A) Representative recordings show $[Ca^{2+}]_i$ measured at room temperature (22°C) using fura-2-based digital imaging as described in Methods. NMDA (20 μM) and glycine (200 μM) were applied in Mg^{2+}-free HHSS for 30 s by superfusion at the time indicated by the horizontal bar. (A) Recordings show traces from cultures pre-incubated for 15 min in Mg^{2+}-free HHSS containing 100 nM TTX and 3 μM CNQX (red line) or Mg^{2+}-free HHSS containing 100 nM TTX, 3 μM CNQX, and 10 μM Bic in the absence (purple line) or added presence of 10 μM NBA (blue line). (B) Bar graph summarizes mean NMDA-evoked $[Ca^{2+}]_i$ responses (AUC) from cultures pre-incubated in Mg^{2+}-free HHSS containing TTX and CNQX (red bar) or Mg^{2+}-free HHSS containing TTX, CNQX and Bic in the absence (purple bar) or presence of NBA (blue bar). One-way ANOVA $F_{(2,18)} = 2.662$, $p = 0.0069$ *$p < 0.05$ with Tukey's post hoc test.

(10 μM). MK801 blocks the NMDA-gated pore of the NMDAR and, as shown in Figure S1, blocked completely the NMDA-evoked increase in $[Ca^{2+}]_i$.

3.5 | BPN Inhibits and NBA Potentiates NMDA-Evoked Increases in $[Ca^{2+}]_i$

We next examined the possibility that the inhibition of NMDA-evoked increases in $[Ca^{2+}]_i$ by BPN might also be sensitive to attenuation by the TRPM4 inhibitor NBA. Cells were pre-incubated in HHSS for 15 min at 22°C without further additions (control) or in the presence of 10 μM BPN, 10 μM NBA, or 10 μM BPN + 10 μM NBA. TTX was applied 2 min before the start of the experiment to reduce spontaneous activity. The initial baseline $[Ca^{2+}]_i$ was similar for all treatment conditions (control = 0.49 ± 0.05 F_{340}/F_{380}; BPN = 0.52 ± 0.12 F_{340}/F_{380}; NBA = 0.48 ± 0.05 F_{340}/F_{380}; BPN + NBA = 0.50 ± 0.04 F_{340}/F_{380}; one way ANOVA: $F_{[3,20]} = 0.0418$, $p = 0.988$). NMDA (20 μM) was applied in Mg^{2+}-free HHSS containing 200 μM glycine to evoke a $[Ca^{2+}]_i$ response (Figure 5A). Consistent with BPN inhibition of I_{NMDA} (Figure 2) and inhibition of NMDA-evoked Ca^{2+} influx (Figure 3), BPN inhibited NMDA-evoked $[Ca^{2+}]_i$ responses under these conditions by 51% ± 16% relative to control. In contrast, NBA treatment increased the magnitude of the NMDA-evoked $[Ca^{2+}]_i$ response by 90% ± 15%. In the presence of both NBA and BPN, the NMDA-evoked $[Ca^{2+}]_i$ response was comparable to control.

TRPM4 is highly sensitive to temperature [10]. All studies described thus far were performed at room temperature (22°C). In Figure 5C,D, we show the results of pharmacological experiments performed at 32°C–34°C. Cells were pre-incubated in HHSS for 15 min in the absence (control) or in the presence of 10 μM BPN, 10 μM NBA, or BPN and NBA together. TTX was applied 2 min before the start of the experiment to reduce spontaneous activity. Superfused buffer was pre-warmed before entering the recording chamber. BPN inhibited the NMDA-evoked $[Ca^{2+}]_i$ response recorded at 32°C–34°C by 42% ± 10% relative to control (Figure 5C,D). This effect was not statistically different from the inhibition observed at room temperature (two-way ANOVA: Effect of BPN $F_{[1,26]} = 28.08$, $p < 0.0001$, effect of temperature $F_{[1,26]} = 10.56$, $p = 0.0032$, BPN × temperature interaction $F_{[1,26]} = 0.0837$, $p = 0.7747$). In contrast, NBA failed to potentiate the NMDA-evoked $[Ca^{2+}]_i$ response at 32°C–34°C. Furthermore, NBA did not attenuate the inhibition produced by BPN. Thus, the effects of NBA are highly sensitive to temperature while the inhibition produced by BPN is robust at room and physiological temperatures.

3.6 | Hyperosmotic Media Inhibits NMDA-Evoked $[Ca^{2+}]_i$ Increases

The potentiation of the NMDA-evoked $[Ca^{2+}]_i$ response by the TRPM4 inhibitor NBA led us to question what effect activation of TRPM4 would have on NMDAR function. Media made hyperosmotic by elevating NaCl activates TRPM4 in HEK293A cells [32]. Thus, we increased the extracellular NaCl concentration to induce osmotic stress as a tool to activate TRPM4 [32]. After loading with fura-2 AM, cells were washed for 15 min in 237 mM NaCl (482 mOsM), Mg^{2+}-free HHSS (High NaCl) containing TTX and CNQX. NMDA (20 μM) and glycine (200 μM) were applied by superfusion to evoke an increase in $[Ca^{2+}]_i$. Pretreatment with high NaCl reduced the magnitude of the NMDA-evoked $[Ca^{2+}]_i$ response by 50% ± 20% (Figure 6A,D). Pretreatment with 10 μM NBA restored the NMDA-evoked $[Ca^{2+}]_i$ response (Figure 6A,D) to a level comparable to control (Figure 5B) (Students *t*-test: $t_{[10]} = 0.07525$, $p = 0.9415$). Pretreatment with 10 μM BPN in the presence of high NaCl did not produce a further reduction

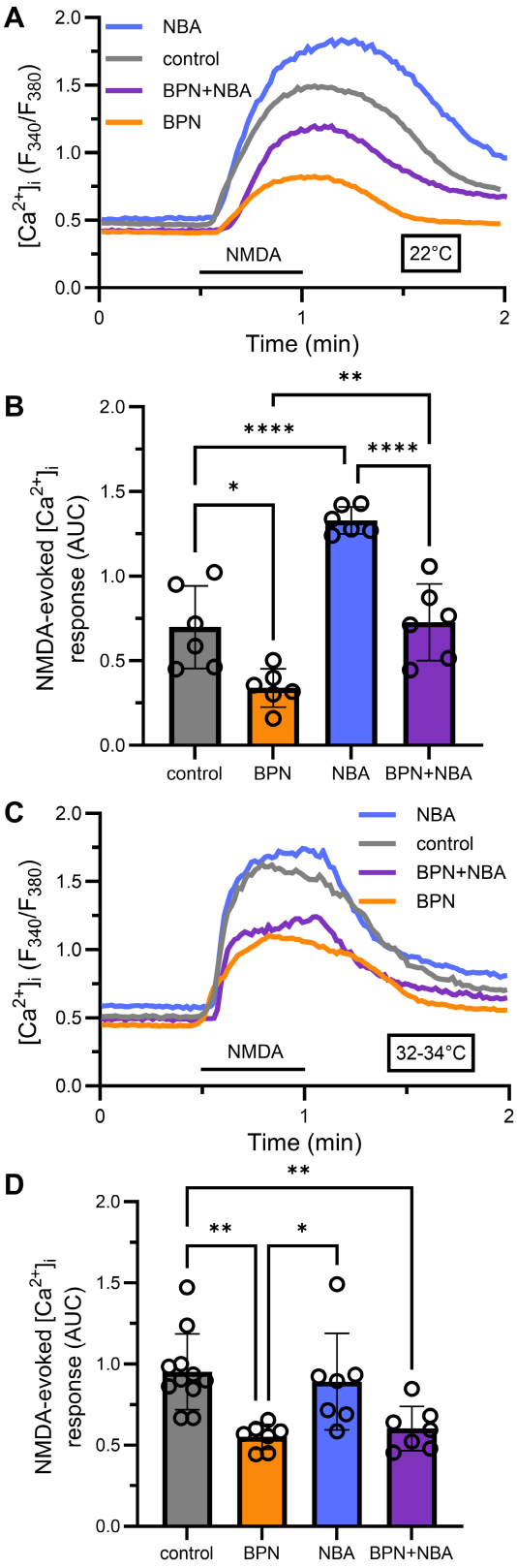

FIGURE 5 | The effects of BPN and NBA on NMDA-evoked increases in $[Ca^{2+}]_i$ recorded at 22°C and 32°C–34°C. (A) Recordings at 22°C from cells pre-incubated in HHSS for 15 min in the absence (control; gray line) or presence of 10 μM BPN (orange line), 10 μM NBA (blue line) or BPN + NBA (purple line) are shown. NMDA (20 μM) and glycine (200 μM) in Mg^{2+}-free HHSS were applied at the time indicated by the horizontal bar. (B) Bar graph summarizes the magnitude of the NMDA-evoked $[Ca^{2+}]_i$ (AUC) responses for replicates of the experiments shown in (A). Two-way ANOVA: Effect of BPN $F_{(1,20)} = 42.38$, $p < 0.0001$, effect of NBA $F_{(1,20)} = 47.76$, $p < 0.0001$, BPN × NBA interaction $F_{(1,20)} = 2.692$, $p = 0.1165$. $^*p < 0.05$, $^{**}p < 0.01$, $^{****}p < 0.0001$ with Tukey's post hoc test. (C) Recordings at 32°C–34°C from cells pre-incubated in HHSS for 15 min in the absence (control; gray line) or presence of 10 μM BPN (orange line), 10 μM NBA (blue line) or BPN + NBA (purple line) are shown. NMDA (20 μM) and glycine (200 μM) in Mg^{2+}-free HHSS were applied at the time indicated by the horizontal bar. (D) Bar graph summarizes the magnitude of the NMDA-evoked $[Ca^{2+}]_i$ (AUC) responses for replicates of the experiments shown in (C). Two-way ANOVA: Effect of BPN $F_{(1,28)} = 21.01$, $p < 0.0001$, effect of NBA $F_{(1,28)} = 0.0041$, $p = 0.9495$, BPN × NBA interaction $F_{(1,28)} = 0.5502$, $p = 0.4644$. $^*p < 0.05$, $^{**}p < 0.01$ with Tukey's post hoc test. Data presented as mean ± SD. Individual points are mean $[Ca^{2+}]_i$ values for all cells in a single field from a single coverslip.

in the magnitude of the NMDA-evoked $[Ca^{2+}]_i$ response relative to high NaCl alone (Figure 6A,D). The retention of fura-2 and the reversal by NBA indicate that the effects of high NaCl did not result from potentially toxic effects of hyperosmotic NaCl. These results suggest that stimuli that activate TRPM4 inhibit Ca^{2+} influx through NMDARs and that this inhibition mimics the effect of BPN.

As TRPM4 is permeable to Na^+, we next examined an increase in extracellular osmolarity without adjusting the NaCl concentration. The addition of mannitol, a sugar alcohol that is not membrane permeable, was used as an alternative method to increase osmolarity [32]. NMDA-evoked $[Ca^{2+}]_i$ responses were recorded after a 15-min pre-incubation in HHSS made hyperosmotic by the addition of 200 mM (474 mOsM) or 300 mM (585 mOsM) mannitol. The addition of mannitol decreased the maximum $[Ca^{2+}]_i$ response by respectively 22% ± 16% and 26% ± 20% relative to the control (Figure 6B,C,E,F), however, this effect was not statistically significant. BPN (10 μM) significantly inhibited the NMDA-evoked response recorded in 200 mM mannitol by 37% ± 13% (Figure 6B,E). NBA increased the NMDA-evoked $[Ca^{2+}]_i$ response in 300 mM by 48% ± 27%, but this effect was not significant (Figure 6C,F). Thus, the effect of mannitol showed a similar trend to that seen in high NaCl, but this effect was not sufficiently robust to reach statistical significance.

4 | Discussion

The NMDAR/TRPM4 complex inhibitor BPN prevents NMDA-induced excitotoxic cell death (Figure 1) [6]. Here we show that BPN inhibits Ca^{2+} flux through NMDARs, providing a mechanism for its neuroprotective properties. In addition, we show that the TRPM4 inhibitor NBA modulates reciprocally the function of NMDARs. In Figure 7, we provide a hypothetical model incorporating the results presented here with published findings showing the NMDAR/TRPM4 complex as the target for novel actions of drugs that act on TRPM4 in neurons.

BPN inhibited currents and $[Ca^{2+}]_i$ increases evoked by NMDA. This effect was not secondary to inhibition of TRPM4-mediated

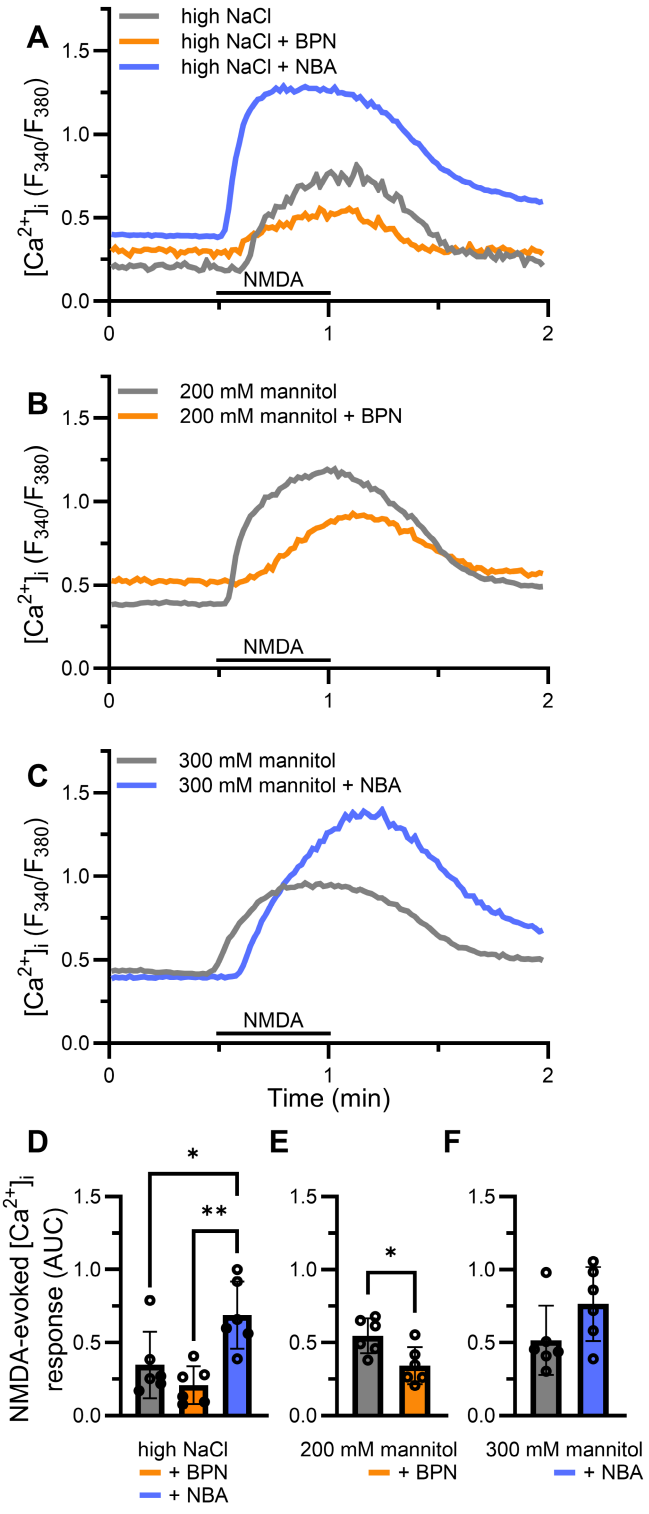

FIGURE 6 | The effects of high NaCl and mannitol on NMDA-evoked increases in $[Ca^{2+}]_i$. (A–C) Representative room temperature (22°C) recordings show $[Ca^{2+}]_i$ measured using fura-2-based digital imaging as described in Methods. NMDA (20 μM) and glycine (200 μM) were applied in hyperosmotic Mg^{2+}-free HHSS for 30 s by superfusion at the time indicated by the horizontal bar. (A) Representative traces are from cells pre-incubated in HHSS with NaCl increased from 140 mM to 240 mM (high NaCl) for 15 min. Traces are from cells pre-incubated with high NaCl alone (gray line) or with the addition of 10 μM BPN (high NaCl + BPN; orange line) or 10 μM NBA (high NaCl + NBA; blue line). (B, C) Representative recordings are from cells pre-incubated in HHSS containing 200 or 300 mM mannitol for 15 min. (B) Traces are from cells pre-incubated with 200 mM mannitol (200 mM mannitol; gray line) or 200 mM mannitol in the presence of 10 μM BPN (200 mM mannitol + BPN; orange line). (C) Traces are from cells pre-incubated with 300 mM mannitol (300 mM mannitol; gray line) or 300 mM mannitol in the presence of 10 μM NBA (300 mM mannitol + NBA; blue line). (D) Bar graph summarizes mean NMDA-evoked $[Ca^{2+}]_i$ responses (AUC) from cultures pre-incubated in HHSS containing high NaCl (gray bar), high NaCl + BPN (orange bar), or high NaCl + NBA (blue bar). One-way ANOVA: $F_{(2,15)} = 8.99$, $p = 0.0027$. *$p < 0.05$, **$p < 0.01$ with Tukey's post hoc test. (E) Bar graph summarizes mean NMDA-evoked $[Ca^{2+}]_i$ responses (AUC) from cultures pre-incubated in HHSS containing 200 mM mannitol (200 mM mannitol; gray bar) or 200 mM mannitol in the presence of 10 μM BPN (200 mM mannitol + BPN; orange bar) Student's *t*-test: $T_{(10)} = 2.86$, $p = 0.0171$. (F) Bar graph summarizes mean NMDA-evoked $[Ca^{2+}]_i$ responses (AUC) from cultures pre-incubated in HHSS containing 300 mM mannitol (300 mM mannitol + NBA; gray bar) or 300 mM mannitol in the presence of 10 μM NBA (300 mM mannitol + NBA; blue bar). Student's *t*-test: $T_{(10)} = -1.766$, $p = 0.108$. Data presented as mean ± SD. Individual points are mean $[Ca^{2+}]_i$ values for all cells in a single field from a single coverslip.

Na^+ influx because BPN was effective in the absence of extracellular Na^+ and with $[Ca^{2+}]_i$ chelated to prevent activation of TRPM4 (Figure 2). Taking into consideration the extensive biochemical studies of Yan et al. [6] showing that TRPM4 forms a complex with NMDARs, and that this complex is disrupted by BPN, the most reasonable explanation for this result is that the formation of the NMDAR/TRPM4 complex markedly potentiates ion flux through activated NMDARs. Because the inhibition of I_{NMDA} by BPN was not dependent on TRPM4-mediated Na^+ flux, we predicted the selective TRPM4 inhibitor NBA would have no effect on NMDA-evoked $[Ca^{2+}]_i$ responses. However, NBA potentiated NMDA-evoked $[Ca^{2+}]_i$ responses, and when BPN and NBA were applied simultaneously, the resulting NMDA-evoked $[Ca^{2+}]_i$ response was equivalent to the control group with no pretreatment (Figure 5). It is possible that NBA and BPN bind simultaneously to TRPM4 eliciting independent effects and thus occlude each other's effects. Alternatively, an equilibrium may exist between NBA bound TRPM4 in complex with NMDARs and BPN bound TRPM4 in which the complex is disrupted. Further studies on how drug binding affects the kinetics of NMDAR/TRPM4 complex formation and dissociation are necessary to draw definite conclusions. The NBA analog CBA has been shown to increase TRPM4 receptor trafficking to the plasma membrane [19]. Thus, NBA may increase TRPM4 trafficking to the surface, while the application of BPN might drive NMDAR sequestration. These scenarios would result in more functional NMDARs in the presence of NBA and fewer cell surface NMDARs in the presence of BPN.

The TRP ion channel family transduces sensory stimuli into electrical and biochemical signals [33]. TRPM4 is modulated by increases in $[Ca^{2+}]_i$ [7], mechanical stress [8], decreases in cellular ATP [9], changes in temperature [11], and binding to phosphatidylinositol 4,5-bisphosphate [33]. Decavanadate and ATP bind to different locations on TRPM4 at physiological versus lower temperatures [10]. Thus, the temperature-dependent

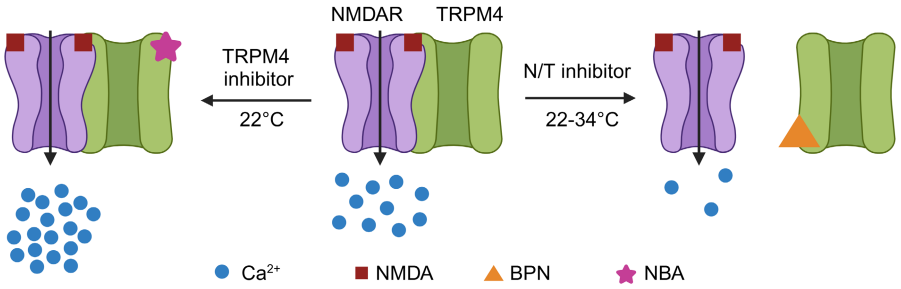

FIGURE 7 | Hypothetical model illustrates the effects of TRPM4 modulation of NMDAR function. Treatment with BPN disrupts the NMDAR/TRPM4 (N/T) complex [6] resulting in impaired Ca^{2+} flux through NMDARs (Figures 2, 3, and 5). In contrast, NBA, which binds to and inhibits TRPM4 [19], potentiates NMDA-evoked Ca^{2+} influx at room temperature (Figure 5).

effects of NBA are consistent with changes to ligand binding sites on TRPM4 by temperature.

The inhibition of NMDA-evoked Ca^{2+} influx produced by Bic may result from osmotic changes because $GABA_AR$ activity can induce swelling of hippocampal neurons [34]. The significance of the effects of Bic, and more generally the cocktail containing TTX, CNQX, and Bic, is that long incubations in buffers containing these channel blockers, which are often used to isolate currents through NMDARs, produce a time-dependent inhibition of NMDA-evoked Ca^{2+} influx that occludes the inhibitory effects of BPN. Thus, we believe recording conditions may account for the lack of effect of BPN on I_{NMDA} in a previous report [6].

The physiological role of TRPM4 in neurons is not entirely clear. We show that linking mechanical stimuli to NMDAR function may be one role. The liquidity of biomolecular condensates is regulated by TRPM4-mediated Na^+ influx in HEK293 cells [32] suggesting a similar response to hyperosmotic stress in neurons might affect NMDAR signaling. Activation of TRPM4 has been associated with traumatic brain injuries and the regulation of osmotic balance [35]. The TRPM4 inhibitor 9-phenanthrol improved outcomes following cerebral edema [15]. Na^+ influx potentiates NMDARs via activation of a Src kinase [36]. Thus, NBA might afford protection from excitotoxicity by reducing TRPM4-mediated Na^+ influx near the NMDAR. Because the potentiation of NMDAR-mediated Ca^{2+} influx by NBA only occurred at non-physiological temperatures, a potentiation of toxicity by this drug would not be anticipated in vivo.

BPN reduced neuronal damage in mice following middle cerebral artery occlusion [6] and FP802, an analog of BPN, reduced loss of motor neurons in a model of ALS [21]. These disorders have a strong excitotoxic component that is attenuated by NMDAR antagonists [37, 38]. NMDAR antagonists developed to date evoke addictive and psychotropic effects in humans at doses that protect from excitotoxicity in animal models [39, 40]. The novel NMDAR/TRPM4 interface inhibitors appear to avoid these adverse effects because the NMDAR/TRPM4 complexes are predominately extrasynaptic [6]. We did not address the question of whether BPN affects synaptic plasticity, although the somatic $[Ca^{2+}]_i$ recordings described here are consistent with a robust effect of BPN on esNMDARs. Knockout of *Trpm4* impaired LTP in a manner reversed by pairing postsynaptic depolarization with presynaptic stimulation, suggesting that a better understanding of the potential role of TRPM4 on synaptic function is needed [14]. Another TRPM family member that binds NMDARs, TRPM2, modulates NMDAR subunit expression in neurons [41]. Perhaps *Trpm4* knockout alters gene expression regulated by esNMDARs resulting in an altered threshold for LTP.

There are limitations to this study. We did not determine the biochemical status of the NMDAR/TRPM4 complex, instead relying on published work to address this question in the case of treatment with BPN [6], and speculating that NBA-bound TRPM4 can form complexes with NMDARs (Figure 7). Determining whether NBA stabilizes the complex to shift the equilibrium towards increased formation of NMDAR/TRPM4 complexes or whether it potentiates NMDA-evoked Ca^{2+} influx by allosteric modulation of existing complexes are interesting questions for future study. We focused on the modulation of NMDAR by drugs acting on TRPM4 and ruled out the possibility that inhibition of NMDAR by BPN required either an elevation of $[Ca^{2+}]_i$ or Na^+ influx. However, understanding how BPN affects TRPM4-mediated Na^+ currents and how NMDAR/TRPM4 complex formation relates to TRPM4 function are also interesting topics for future research. Of particular interest will be determining if inhibition of NMDA-evoked increases in $[Ca^{2+}]_i$ by stimuli that activate TRPM4 require Na^+ flux to affect NMDAR function. TRPM2 potentiates NMDAR function by bringing protein kinase Cγ (PKCγ) in close proximity to the NMDAR when complexed; Ca^{2+} influx via TRPM2 contributes to the activation of PKCγ [42]. We are not aware of a precedent for TRP channels acting as detectors of sensory stimuli independent of their ion channel activity. We did not determine the contribution of metabotropic NMDAR signaling [43] to the cell death evoked by NMDA in the neurotoxicity assay (Figure 1). Understanding how TRPM4 affects metabotropic relative to ionotropic NMDAR signaling might guide the use and development of neuroprotective agents.

Therapies disrupting the NMDAR/TRPM4 complex have already shown success in rodent models of disease involving NMDAR-mediated excitotoxicity [6, 21]. We found that NMDAR/TRPM4 interface inhibitor BPN inhibited Ca^{2+} flux through NMDARs providing a mechanism for the neuroprotective effects of BPN. Thus, drugs and stimuli that modulate TRPM4 provide a new route to regulate NMDAR function. Future studies aimed at understanding how the NMDAR/TRPM4 complex is regulated by physiological and pathological stimuli will aid in the development of drugs to selectively modulate NMDARs.

Author Contributions

Participated in research design: J. Casby, B. Gansemer, S. Thayer. Conducted experiments: J. Casby, B. Gansemer. Performed data analysis: J. Casby, B. Gansemer. Wrote or contributed to the writing of the manuscript: J. Casby, B. Gansemer, S. Thayer.

Acknowledgments

We thank Rachel Allen for help with $[Ca^{2+}]_i$ recordings. Figure 7 was created with BioRender.com.

Conflicts of Interest

The authors declare no conflicts of interest.

Data Availability Statement

All data are available upon request.

References

1. H. Ma, H. G. Khaled, X. Wang, et al., "Excitation-Transcription Coupling, Neuronal Gene Expression and Synaptic Plasticity," *Nature Reviews. Neuroscience* 24, no. 11 (2023): 672–692, https://doi.org/10.1038/s41583-023-00742-5.

2. R. G. Mira and W. Cerpa, "Building a Bridge Between NMDAR-Mediated Excitotoxicity and Mitochondrial Dysfunction in Chronic and Acute Diseases," *Cellular and Molecular Neurobiology* 41, no. 7 (2021): 1413–1430, https://doi.org/10.1007/s10571-020-00924-0.

3. P. Vanhoutte and H. Bading, "Opposing Roles of Synaptic and Extrasynaptic NMDA Receptors in Neuronal Calcium Signalling and BDNF Gene Regulation," *Current Opinion in Neurobiology* 13, no. 3 (2003): 366–371.

4. G. E. Hardingham, Y. Fukunaga, and H. Bading, "Extrasynaptic NMDARs Oppose Synaptic NMDARs by Triggering CREB Shut-Off and Cell Death Pathways," *Nature Neuroscience* 5, no. 5 (2002): 405–414, https://doi.org/10.1038/nn835.

5. K. Haddow, P. C. Kind, and G. E. Hardingham, "NMDA Receptor C-Terminal Domain Signalling in Development, Maturity, and Disease," *International Journal of Molecular Sciences* 23, no. 19 (2022): 11392, https://doi.org/10.3390/ijms231911392.

6. J. Yan, C. P. Bengtson, B. Buchthal, A. M. Hagenston, and H. Bading, "Coupling of NMDA Receptors and TRPM4 Guides Discovery of Unconventional Neuroprotectants," *Science* 370, no. 6513 (2020): eaay3302, https://doi.org/10.1126/science.aay3302.

7. B. Nilius, J. Prenen, J. Tang, et al., "Regulation of the Ca^{2+} Sensitivity of the Nonselective Cation Channel TRPM4," *Journal of Biological Chemistry* 280, no. 8 (2005): 6423–6433, https://doi.org/10.1074/jbc.M411089200.

8. S. Yoo, D. R. Mittelstein, R. C. Hurt, J. Lacroix, and M. G. Shapiro, "Focused Ultrasound Excites Cortical Neurons via Mechanosensitive Calcium Accumulation and Ion Channel Amplification," *Nature Communications* 13, no. 1 (2022): 493, https://doi.org/10.1038/s41467-022-28040-1.

9. J. M. Simard, S. K. Woo, and V. Gerzanich, "Transient Receptor Potential Melastatin 4 and Cell Death," *Pflügers Archiv* 464, no. 6 (2012): 573–582, https://doi.org/10.1007/s00424-012-1166-z.

10. J. Hu, S. J. Park, T. Walter, et al., "Physiological Temperature Drives TRPM4 Ligand Recognition and Gating," *Nature* 630 (2024): 509–515, https://doi.org/10.1038/s41586-024-07436-7.

11. K. Talavera, K. Yasumatsu, T. Voets, et al., "Heat Activation of TRPM5 Underlies Thermal Sensitivity of Sweet Taste," *Nature* 438, no. 7070 (2005): 1022–1025, https://doi.org/10.1038/nature04248.

12. A. Borgstrom, C. Peinelt, and P. Stoklosa, "TRPM4 in Cancer-A New Potential Drug Target," *Biomolecules* 11, no. 2 (2021): 229, https://doi.org/10.3390/biom11020229.

13. F. Vandewiele, A. Pironet, G. Jacobs, et al., "TRPM4 Inhibition by Meclofenamate Suppresses Ca^{2+}-Dependent Triggered Arrhythmias," *European Heart Journal* 43, no. 40 (2022): 4195–4207, https://doi.org/10.1093/eurheartj/ehac354.

14. A. Menigoz, T. Ahmed, V. Sabanov, et al., "TRPM4-Dependent Post-Synaptic Depolarization Is Essential for the Induction of NMDA Receptor-Dependent LTP in CA1 Hippocampal Neurons," *Pflügers Archiv* 468, no. 4 (2016): 593–607, https://doi.org/10.1007/s00424-015-1764-7.

15. P. Ma, N. Huang, J. Tang, et al., "The TRPM4 Channel Inhibitor 9-Phenanthrol Alleviates Cerebral Edema After Traumatic Brain Injury in Rats," *Frontiers in Pharmacology* 14 (2023): 1098228, https://doi.org/10.3389/fphar.2023.1098228.

16. T. T. Dundar, A. Abdallah, I. Yurtsever, E. M. Guler, O. F. Ozer, and O. Uysal, "Serum SUR1 and TRPM4 in Patients With Subarachnoid Hemorrhage," *Neurosurgical Review* 43, no. 6 (2020): 1595–1603, https://doi.org/10.1007/s10143-019-01200-6.

17. B. Bianchi, P. A. Smith, and H. Abriel, "The Ion Channel TRPM4 in Murine Experimental Autoimmune Encephalomyelitis and in a Model of Glutamate-Induced Neuronal Degeneration," *Molecular Brain* 11, no. 1 (2018): 41, https://doi.org/10.1186/s13041-018-0385-4.

18. C. Delalande, M. Awale, M. Rubin, et al., "Optimizing TRPM4 Inhibitors in the MHFP6 Chemical Space," *European Journal of Medicinal Chemistry* 166 (2019): 167–177, https://doi.org/10.1016/j.ejmech.2019.01.048.

19. L. C. Ozhathil, C. Delalande, B. Bianchi, et al., "Identification of Potent and Selective Small Molecule Inhibitors of the Cation Channel TRPM4," *British Journal of Pharmacology* 175, no. 12 (2018): 2504–2519, https://doi.org/10.1111/bph.14220.

20. P. Arullampalam, B. Preti, D. Ross-Kaschitza, M. Lochner, J. S. Rougier, and H. Abriel, "Species-Specific Effects of Cation Channel TRPM4 Small-Molecule Inhibitors," *Frontiers in Pharmacology* 12 (2021): 712354, https://doi.org/10.3389/fphar.2021.712354.

21. J. Yan, Y. M. Wang, A. Hellwig, and H. Bading, "TwinF Interface Inhibitor FP802 Stops Loss of Motor Neurons and Mitigates Disease Progression in a Mouse Model of ALS," *Cell Reports Medicine* 5, no. 2 (2024): 101413, https://doi.org/10.1016/j.xcrm.2024.101413.

22. M. V. Green and A. E. West, "TRPing Into Excitotoxic Neuronal Death," *Cell Calcium* 93 (2021): 102331, https://doi.org/10.1016/j.ceca.2020.102331.

23. X. Zhang, M. V. Green, and S. A. Thayer, "HIV gp120-Induced Neuroinflammation Potentiates NMDA Receptors to Overcome Basal Suppression of Inhibitory Synapses by p38 MAPK," *Journal of Neurochemistry* 148, no. 4 (2019): 499–515, https://doi.org/10.1111/jnc.14640.

24. H. J. Kim, A. H. Shin, and S. A. Thayer, "Activation of Cannabinoid Type 2 Receptors Inhibits HIV-1 Envelope Glycoprotein gp120-Induced Synapse Loss," *Molecular Pharmacology* 80, no. 3 (2011): 357–366, https://doi.org/10.1124/mol.111.071647.

25. M. V. Green and S. A. Thayer, "NMDARs Adapt to Neurotoxic HIV Protein Tat Downstream of a GluN2A-Ubiquitin Ligase Signaling Pathway," *Journal of Neuroscience* 36 (2016): 12640–12649, https://doi.org/10.1523/JNEUROSCI.2980-16.2016.

26. R. Schneggenburger, "Simultaneous Measurement of Ca^{2+} Influx and Reversal Potentials in Recombinant N-Methyl-D-Aspartate Receptor Channels," *Biophysical Journal* 70, no. 5 (1996): 2165–2174, https://doi.org/10.1016/s0006-3495(96)79782-5.

27. K. K. Krogh and S. A. Thayer, "$[Ca^{2+}]_i$ Imaging to Study Glutamate Receptor-Mediated Cellular Responses," in *Ionotropic Glutamate Receptor Technologies*, ed. G. K. Popescu (New York, NY: Springer Science+Business Media, 2015), 83–101.

28. S. A. Thayer, M. Sturek, and R. J. Miller, "Measurement of Neuronal Ca^{2+} Transients Using Simultaneous Microfluorimetry and Electrophysiology," *Pflügers Archiv* 412, no. 1–2 (1988): 216–223.

29. Y. Li, J. Popko, K. A. Krogh, and S. A. Thayer, "Epileptiform Stimulus Increases Homer 1a Expression to Modulate Synapse Number and Activity in Hippocampal Cultures," *Journal of Neurophysiology* 28, no. 130 (2013): 1494–1504.

30. S. D. Harding, J. L. Sharman, E. Faccenda, et al., "The IUPHAR/BPS Guide to PHARMACOLOGY in 2019: Updates and Expansion to Encompass the New Guide to IMMUNOPHARMACOLOGY," *Nucleic Acids Research* 46 (2018): D1091–D1106, https://doi.org/10.1093/nar/gkx1121.

31. S. P. H. Alexander, A. A. Mathie, J. A. Peters, et al., "The Concise Guide to PHARMACOLOGY 2023/24: Ion Channels," *British Journal of Pharmacology* 180 (2023): S145–S222, https://doi.org/10.1111/bph.16178.

32. K. Morishita, K. Watanabe, I. Naguro, and H. Ichijo, "Sodium Ion Influx Regulates Liquidity of Biomolecular Condensates in Hyperosmotic Stress Response," *Cell Reports* 42, no. 4 (2023): 112315, https://doi.org/10.1016/j.celrep.2023.112315.

33. E. R. Liman, "TRPM5 and Taste Transduction," *Handbook of Experimental Pharmacology* 179 (2007): 287–298, https://doi.org/10.1007/978-3-540-34891-7_17.

34. S. Takagi, K. Obata, and H. Tsubokawa, "GABAergic Input Contributes to Activity-Dependent Change in Cell Volume in the Hippocampal CA1 Region," *Neuroscience Research* 44, no. 3 (2002): 315–324, https://doi.org/10.1016/s0168-0102(02)00153-0.

35. Z. Zheng, Z. Qiu, X. Xiong, et al., "Co-Activation of NMDAR and mGluRs Controls Protein Nanoparticle-Induced Osmotic Pressure in Neurotoxic Edema," *Biomedicine & Pharmacotherapy* 169 (2023): 115917, https://doi.org/10.1016/j.biopha.2023.115917.

36. X. M. Yu and M. W. Salter, "Gain Control of NMDA-Receptor Currents by Intracellular Sodium," *Nature* 396, no. 6710 (1998): 469–474.

37. Z. Shen, M. Xiang, C. Chen, et al., "Glutamate Excitotoxicity: Potential Therapeutic Target for Ischemic Stroke," *Biomedicine & Pharmacotherapy* 151 (2022): 113125, https://doi.org/10.1016/j.biopha.2022.113125.

38. P. Paul and J. de Belleroche, "The Role of D-Serine and Glycine as Co-Agonists of NMDA Receptors in Motor Neuron Degeneration and Amyotrophic Lateral Sclerosis (ALS)," *Frontiers in Synaptic Neuroscience* 6 (2014): 10, https://doi.org/10.3389/fnsyn.2014.00010.

39. K. K. Ogden and S. F. Traynelis, "New Advances in NMDA Receptor Pharmacology," *Trends in Pharmacological Sciences* 32, no. 12 (2011): 726–733, https://doi.org/10.1016/j.tips.2011.08.003.

40. K. W. Muir, "Glutamate-Based Therapeutic Approaches: Clinical Trials With NMDA Antagonists," *Current Opinion in Pharmacology* 6, no. 1 (2006): 53–60, https://doi.org/10.1016/j.coph.2005.12.002.

41. I. Alim, L. Teves, R. Li, Y. Mori, and M. Tymianski, "Modulation of NMDAR Subunit Expression by TRPM2 Channels Regulates Neuronal Vulnerability to Ischemic Cell Death," *Journal of Neuroscience* 33, no. 44 (2013): 17264–17277, https://doi.org/10.1523/jneurosci.1729-13.2013.

42. P. Zong, J. Feng, N. Legere, et al., "TRPM2 Enhances Ischemic Excitotoxicity by Associating With PKCγ," *Cell Reports* 43, no. 2 (2024): 113722, https://doi.org/10.1016/j.celrep.2024.113722.

43. N. L. Weilinger, A. W. Lohman, B. D. Rakai, et al., "Metabotropic NMDA Receptor Signaling Couples Src Family Kinases to Pannexin-1 During Excitotoxicity," *Nature Neuroscience* 19, no. 3 (2016): 432–442, https://doi.org/10.1038/nn.4236.

Supporting Information

Additional supporting information can be found online in the Supporting Information section.